www.czasopisma.pan.pl PAN POLSKA AKADEMIA NAUK www.journals.pan.pl

Arch. Metall. Mater. **65** (2020), 3, 1001-1004

DOI: 10.24425/amm.2020.133206

SEUNGGYU CHOI[1], JUNHYUB JEON[1], NAMHYUK SEO[1],
YOUNG HOON MOON[2], IN-JIN SHON[1], SEOK-JAE LEE[1*]

EFFECT OF COMPOSITION ON STRAIN-INDUCED MARTENSITE TRANSFORMATION OF FeMnNiC ALLOYS FABRICATED BY POWDER METALLURGY

We investigated the austenite stability and mechanical properties in FeMnNiC alloy fabricated by spark plasma sintering. The addition of Mn, Ni, and C, which are known austenite stabilizing elements, increases its stability to a stable phase existing above 910°C in pure iron; as a result, austenitic microstructure can be observed at room temperature, depending on the amounts of Mn, Ni, and C added. Depending on austenite stability and the volume fraction of austenite at a given temperature, strain-induced martensite transformation during plastic deformation may occur. Both stability and the volume fraction of austenite can be controlled by several factors, including chemical composition, grain size, dislocation density, and so on. The present study investigated the effect of carbon addition on austenite stability in FeMnNi alloys containing different Mn and Ni contents. Microstructural features and mechanical properties were analyzed with regard to austenite stability.

Keywords: FeMnNiC alloy, spark plasma sintering, strain-induced martensite, austenite stability, hardness

1. Introduction

Third-generation advanced high strength steel (AHSS) and its processes has recently been the subject of close attention due to the possibilities it offers both for improving mechanical properties and reducing product costs. Quenching and partitioning (Q&P) steel and medium Mn transformation induced plasticity (TRIP) steel are well-known examples of these third-generation AHSS steels. A common mechanism for improving both strength and ductility in third-generation steels uses strain-induced martensite, transformed from austenite retained at room temperature during deformation [1,2]. The stability of austenite determines the kinetics of the strain-induced martensite transformation and contributes to mechanical properties. Austenite stability is controlled by several factors. The addition of a stabilizing element such as Mn, Ni, or C is widely used to control austenite stability [3,4]. Similarly, a change in grain size change can affect austenite stability. Lee et al. [5] have reported that the fraction of retained austenite was increased by reducing grain size to under 300 nm in ultra-fine grained TRIP steel containing 6 wt.% Mn. Takaki et al. [6] have reported that grain refinement of austenite to 1 μm or less is highly effective in restraining martensitic transformation from fcc structure. Austenite stability can thus be increased when its grain size is decreased, without the addition of other austenite stabilizing elements. However, conventional metal-making processes involving casting, hot forging, or hot rolling show limitations in producing steels with ultra-fine grains under 100 nm.

Powder metallurgy can rise above the limitations of grain refinement by conventional processes. The mechanical alloying (MA) process effectively reduces powder size and obtains nanosized crystallites [7,8]. Since grain growth occurs during sintering, spark plasma sintering (SPS) is an adequate method to complete sintering within a short heating time and to obtain very small grain and crystallite sizes [9-11]. In the present study, we fabricated FeMnNiC alloy powders by high-energy ball mill and obtained nanocrystalline FeMnNiC alloy samples using SPS. The volume fraction of austenite resulting from the stabilizing elements of Mn, Ni, and C was quantitatively analyzed. In addition, the variation in austenite volume fraction during deformation due to strain-induced martensite transformation was also examined in relation to austenite stability. Finally, we propose an equation for predicting the hardness of sintered FeMnNiC alloys.

[1] JEONBUK NATIONAL UNIVERSITY, DIVISION OF ADVANCED MATERIALS ENGINEERING, 567 BAEKJE-DAERO, DEOKJIN-GU, JEONJU, 54896, REPUBLIC OF KOREA
[2] PUSAN NATIONAL UNIVERSITY, SCHOOL OF MECHANICAL ENGINEERING, 2, BUSANDAEHAK-RO 63BEON-GIL, GEUMJEONG-GU, BUSAN, 46241, REPUBLIC OF KOREA

* Corresponding author: seokjaelee@jbnu.ac.kr

2. Experimental

Four Fe-Mn-Ni alloy powders were prepared using a high energy ball mill: Fe-2%Mn-6%Ni, Fe-2%Mn-6%Ni-0.5%C, Fe-4%Mn-11%Ni, and Fe-4%Mn-11%Ni-0.5%C (in wt.%). Fe powder (Alfa Aesar, Korea) of 99% purity and an average particle size of <74 μm, Mn powder (Alfa Aesar, Korea) of 99.6% purity and an average particle size of <10 μm, Ni powder (Alfa Aesar, Korea) of 99.9% purity and an average particle size of <7 μm, and graphite powder of 99% purity and a typical particle size of 7-11 μm were used. Stearic acid ($CH_3(CH_2)_{16}CO_2H$, Alfa Aesar, Korea) was used as process control agent. Mechanical alloying was carried out at 250 rpm for 24 h in an Ar atmosphere using a high-energy ball mill (Fritsch, Pulverisette-5, oil milling) and the ball-to-powder ratio was set at 30:1. A stainless container and a tungsten carbide ball of diameter 10 mm were used. The balance between cold welding and fracturing was controlled by adding 1 wt.% of Stearic acid. The milled alloy powder was poured into a cylindrical graphite mold with an inner diameter of 10 mm, an outer diameter of 35 mm, and a height of 40 mm, sintered by using SPS. The powder sample was heated to 1,000°C in one minute under a high vacuum of under 150 mTorr and uniaxial pressure of 80 MPa, immediately followed by cooling to room temperature. Ten specimens were prepared for each alloy component and analyzed as follows. XRD (X-ray diffraction, Rigaku Co., Max-2500) analysis for phase analysis was carried out with a Cu Kα target at a range of 2θ = 30-100º with a rate of 2º/min. Compressive test specimens of diameter 4mm and height 4mm were prepared from the sintered alloys. The compressive test were performed at a speed of 1×10^{-3} s^{-1} by a universal testing machine (Instron 5569). The Vickers hardness test was performed using a Digital Micro Hardness Tester (TIME Co., TH715).

3. Results and discussion

Fig. 1 shows the XRD results of the FeMnNiC alloy powder prepared using with a high energy ball mill. Only bcc α-Fe peaks were observed in the alloy powders. No peak related to Mn and Ni appeared. The maximum solubility of Mn in Fe is reported to be 30 wt.% [12]. The maximum solubility of Ni in Fe is only 4.7 at.%, but it can be increased to 36 at.% by mechanical milling [13]. The lattice strain and crystallite size of the powder was calculated by the Williamson and Hall equation using Bragg angles and full width at half maximum (FWHM) at the XRD peak as follows [14]:

$$B_r \cos\theta = \frac{k\cdot\lambda}{D} + \eta \sin\theta \qquad (1)$$

where B_r is the FWHM of the powder's XRD peak, θ is the Bragg angle, k is the constant, λ is the wavelength of Cu Kα target, D is the crystallite size and η is the lattice strain. The lattice strain and crystallite size of the alloy powder were 0.2-0.4% and 8-12 nm respectively.

Fig. 2 shows the XRD peak of the as-sintered and 20% deformed FeMnNiC alloy samples. The peak intensities of γ (111), γ (200), γ (220) austenite increased when increasing the content of Mn, Ni, and C additions. The volume fraction of each phase was calculated from the XRD intensities based on the Averbach and Cohen method [15]. Changes in the volume fraction of austenite by compressive strain are summarized in Table 1. It was confirmed that the volume fraction of austenite decreased after deformation according to the strain-induced martensite transformation [16]. The increase in the volume fraction of strain-induced martensite during the deformation was influenced by austenite

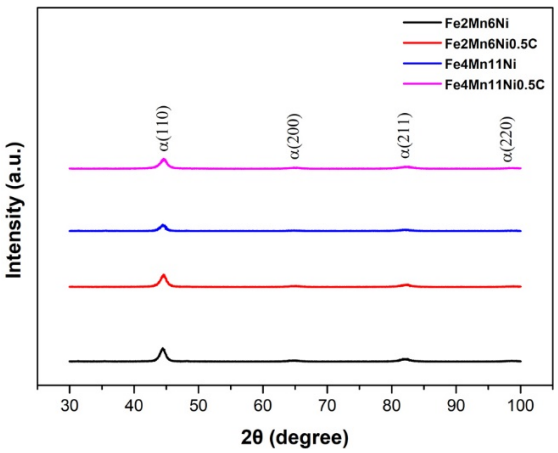

Fig. 1. XRD patterns of the milled FeMnNiC powders

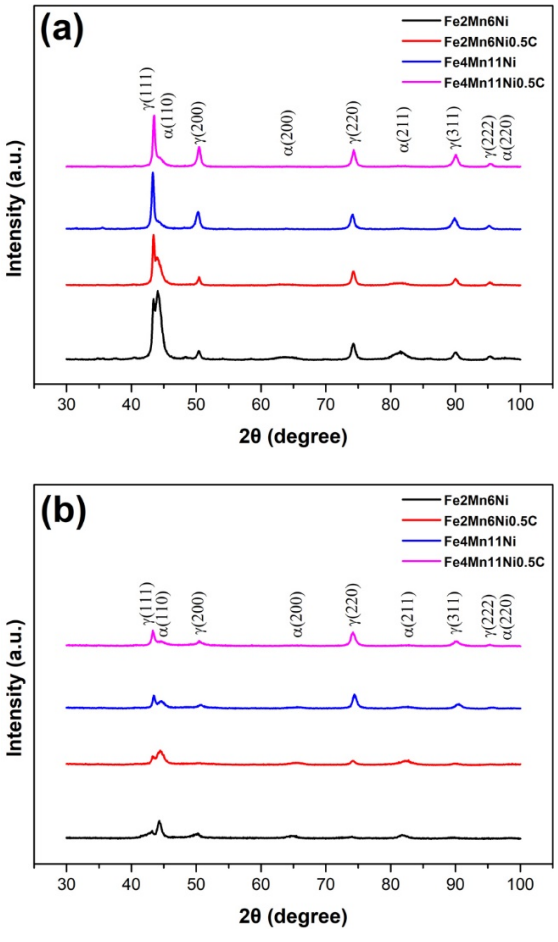

Fig. 2. XRD patterns of the FeMnNiC sintered alloys: (a) as-sintered (b) after 20% compressive deformation

stability. A volume fraction of 33.94 vol.% of austenite was transformed in the Fe2Mn6Ni alloy, whereas a volume fraction of only 2.55 vol.% was transformed in the Fe4Mn11Ni0.5C alloy. The higher the concentration of austenite stabilizing elements such as Mn, Ni, and C, the greater was austenite stability, which plays a role in restricting transformation behavior from austenite to strain-induced martensite during deformation [17].

TABLE 1

Change in the volume fraction of austenite

Alloy	Measured volume fraction of austenite (vol.%)		
	As-sintered	20% deformed	$\Delta\gamma$
Fe2Mn6Ni	72.53 ± 2.18	38.59 ± 1.48	–33.94 ± 5.21
Fe2Mn6Ni0.5C	86.85 ± 2.02	57.20 ± 2.59	–29.65 ± 3.68
Fe4Mn11Ni	94.48 ± 0.45	87.67 ± 0.33	–6.81 ± 0.43
Fe4Mn11Ni0.5C	95.88 ± 0.46	93.33 ± 0.51	–2.55 ± 0.41

The effect of the alloying elements addition on austenite stability was evaluated quantitatively by applying a model for the strain-induced martensite transformation. We adopted the kinetics model proposed by Burke et al. [18], Matsumura et al. [19], and Tsuchida [20]. This BMT model has been used to investigate the strain-induced martensite kinetics in sintered Fe-based alloys in previous studies [17,21,22]. The BMT model used in this study is as follows:

$$V_{\alpha'} = \frac{V_\gamma^0}{1 + p/\left(k\varepsilon^p V_\gamma^0\right)} \tag{2}$$

where $V_{\alpha'}$ is the fraction of the strain-induced martensite, V_γ^0 is the fraction of initial austenite, p is a constant of autocatalytic effect. When autocatalytic effect is zero, p value is 1. It has been reported that the martensite transformation kinetics can be accelerated by decreasing austenite grain size [17,21,22]. The actual grain size of the sintered Fe-based alloy sample produced by high energy ball milling and SPS could be smaller than 30 nm [17,21,22]; the p value was thus decided as 2 for the purposes of this study. ε is the plastic strain, k the constant related to austenite stability. The lower the value of k, the higher the austenite stability. Fig. 3 shows the calculated k value of the sintered FeMnNiC alloy samples using the BMT model. As expected, k value decreases as the amount of Mn, Ni, and C increases, since these are known austenite stabilizers. Note that not only the addition of the austenite stabilizing element but also the volume fraction of austenite prior to transformation is influenced the transformation kinetics of strain-induced martensite. According to Eq. (2) the k value should be lowered, since the V_γ^0 value is increased when an identical volume fraction of strain-induced martensite is assumed.

Microstructural change directly influences mechanical properties. The hardness of the sintered FeMnNiC alloys was varied after the deformation and is compared in Table 2. The increment in hardness in the Fe2Mn6Ni alloy sample was +202 Hv, while in the Fe4Mn11Ni0.5C alloy sample it was only +18 Hv. This can be explained by the absolute volume fraction of

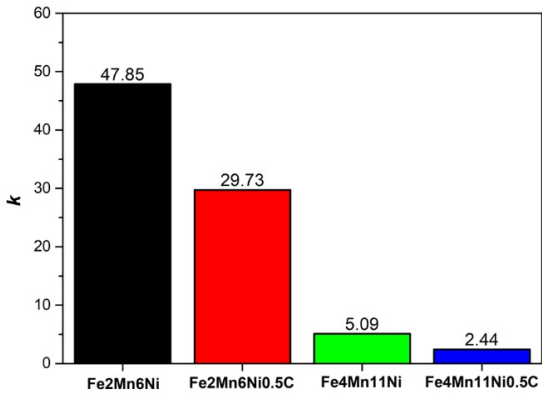

Fig. 3. Calculated k value of sintered FeMnNiC alloys

strain-induced martensite formed during compressive deformation. Fig. 4 shows hardness change compared with the decreased volume fraction of austenite. The increment in hardness shows a tendency similar to the decrease in the austenite volume fraction. It is believed that of hardness change is also a good measure of austenite stability, so austenite stability indicated as the k value in Eq. (2) can be quantitatively evaluated not by calculating the model but by measuring hardness values.

TABLE 2

Vickers hardness change of the FeMnNiC alloy samples with deformation

Alloy	Vickers hardness (H_V)		
	As-sintered	20% deformed	ΔHv
Fe2Mn6Ni	598 ± 7	800 ± 16	202 ± 8
Fe2Mn6Ni0.5C	324 ± 14	400 ± 21	76 ± 8
Fe4Mn11Ni	258 ± 8	279 ± 18	21 ± 16
Fe4Mn11Ni0.5C	296 ± 5	314 ± 7	18 ± 17

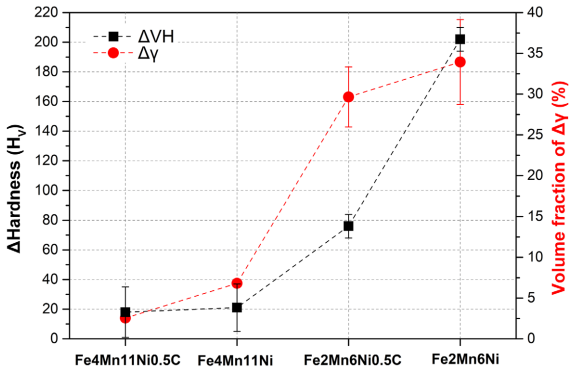

Fig. 4. Variation in hardness compared with decreased volume fraction of austenite after compressive deformation

It is well known that hardness increases with the addition of alloying elements, due to the solid solution strengthening effect [23]. It has also been reported that hardness increases with decreasing grain size and increasing martensite fraction [24]. We accordingly propose an empirical model for predicting the hardness of the sintered FeMnNiC alloy, that considers alloy composition effect, grain size effect, and microstructure

effect as follows:

$$H_V = \alpha + (H_a + H_{gb}) \times f_{(1-\gamma)} \quad (3)$$

where H_V is the Vickers hardness, α is the constant (= 99). $f_{(1-\gamma)}$ is the volume fraction of strain-induced martensite. The alloying element effect (H_a) is given by

$$H_a = 360 + 0.1C_C + 772C_{Mn} + 0.1C_{Ni} \quad (4)$$

where C_i is the concentration of alloying element i in wt.% (i = C, Mn, Ni). The strength effect related to grain size (H_{gb}) is expressed based on the Hall-Petch relationship [25], as follows:

$$H_{gb} = k_0 d^{-1/2} \quad (5)$$

where k_0 is the material constant (= 0.1) and d means the actual grain size equal to the crystalline size, which is calculated by Eq. (1). Fig. 5 shows hardness values as a function of the austenite stability parameter k in Eq. (2). The predicted hardness using Eq. (3) closely matches the measured values. The hardness prediction equation newly proposed in this study can be applied to other alloys, including the strain-induced martensite formation during deformation, and can be used to design alloys effectively.

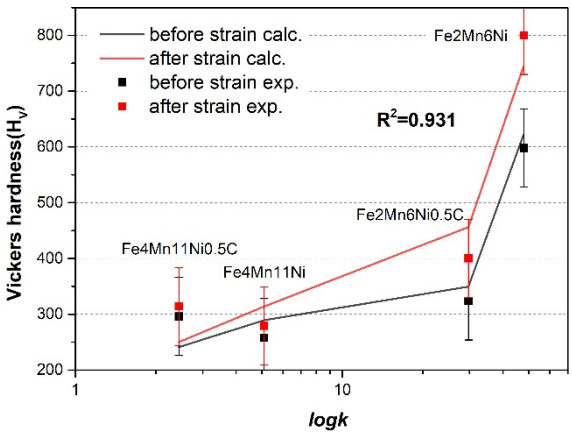

Fig. 5. Relationship between the austenite stability parameter k and hardness values

4. Conclusions

In the present study, we investigated the effect of the addition of Mn, Ni, and C on the strain-induced martensite transformation with regard to the austenite stability of nanocrystalline FeMnNiC alloys fabricated using high energy ball milling and spark plasma sintering. The calculated crystallite size, which acts like the actual grain size of milled alloy powders, was around 10±2 nm, and an austenite volume fraction higher than 72 vol.% was obtained at room temperature. Increasing the content of the austenite stabilizing elements Mn, Ni, and C, led to a corresponding increase in austenite stability, as well as suppressing the transformation kinetics of strain-induced martensite. The variation in austenite stability varied with deformation was quantitatively evaluated using the BMT model. A new empirical equation for predicting hardness was proposed that takes into account the effects of composition, grain size, and microstructure. Finally, the relationship between the austenite stability parameter k and hardness measurement was analyzed.

Acknowledgments

This research was supported by the Basic Science Research program through the National Research Foundation of Korea (NRF), funded by the Ministry of Education (2016R1A1B03935163). It also received financial support from the Ministry of Trade, Industry and Energy (MOTIE) and Korea Institute for Advancement of Technology (KIAT), through the International Cooperative R&D program (P006837).

REFERENCES

[1] S. Lee, S.J. Lee, S.S. Kumar, K. Lee, B.C. De Cooman, Metall. Mater. Trans. A. **42A**, 3638 (2011).
[2] B.C. De Cooman, Curr. Opin. Solid State Mater. Sci. **8**, 285 (2004).
[3] Y. Sakuma, O. Matsumura, H. Takechi, Met. Trans. A. **22**, 489 (1991).
[4] L. Samek, E. De Moor, J. Penning, B.C. De Cooman, Metall. Mater. Trans. A. **37A**, 109 (2006).
[5] S.J. Lee, S. Lee, B.C. De Cooman, Int. J. Mater. Res. **104**, 423 (2013).
[6] S. Takaki, K. Fukunaga, J. Syarif, T. Tsuchiyama, Mater. Trans. **45**, 2245 (2004).
[7] C. Suryanarayana, Prog. Mater. Sci. **46**, 1 (2001).
[8] C. Suryanarayana, E. Ivanov, V.V. Boldyrev, Mater. Sci. Eng. A. **304**, 151 (2001).
[9] M. Omori, Mater. Sci. Eng. A. **287**, 183 (2000).
[10] S.I. Cha, S.H. Hong, B.K. Kim, Mater. Sci. Eng. A. **351**, 31 (2003).
[11] H.W. Zhang, R. Gopalan, T. Mukai, K. Hono, Scripta Mater. **53**, 863 (2005).
[12] H. Hermawan, H. Alamdari, D. Mantovani, D. Dubé, Powder Met. **51**, 38 (2008).
[13] V. Hays, R. Marchand, G. Saindrenan, E. Gaffet, Nanostruct. Mater. **7**, 411 (1996).
[14] G.K. Williamson, W.H. Hall, Acta Metall. **1**, 22 (1953).
[15] B.L. Averbach, M. Cohen, Trans. AIME. **196**, 1 (1948).
[16] P.C. Maxwell, A. Goldberg, J.C. Shyne, Metall. Trans. **5**, 1305 (1974).
[17] S.J. Oh, B.C. Kim, M.C. Suh, I.J. Shon, S.J. Lee, Arch. Metall. Mater. **64**, 863 (2019).
[18] J. Burke, Kinetics of Phase Transformation in Metals, Pergamon Press, Oxford, United Kingdom, 1965.
[19] O. Matsumura, Y. Sakuma, H. Takechi, Scr. Mater. **21**, 1301 (1987).
[20] N. Tsuchida, Y. Tomota, Mater. Sci. Eng. A. **285**, 345 (2000).
[21] D. Park, S.J. OH, I.J. Shon, S.J. Lee, Arch. Metall. Mater. **63**, 1479 (2018).
[22] S.J. Oh, D. Park, K. Kim, I.J. Shon, S.J. Lee, Mater. Sci. Eng. A. **725**, 382 (2018).
[23] W.F. Wang, Mater. Sci. Eng. A. **402**, 92 (2005).
[24] M. Eskandari, A. Najafizadeh, A. Kermanpur, Mater. Sci. Eng. A. **519**, 46 (2009).
[25] K. He, X. Li, M. Guan, S. Qu, X. Yang, J. Zhang, Int. J. Refract. Met. Hard Mater. **58**, 117 (2016).